

Repository Istituzionale dei Prodotti della Ricerca del Politecnico di Bari

Vertical dense jet in flowing current

This is a post print of the following article

Original Citation:
Vertical dense jet in flowing current / Ben Meftah, M., Malcangio, D., De Serio, F., Mossa, M.. - In: ENVIRONMENTAL FLUID MECHANICS. - ISSN 1567-7419. - 18:1(2018), pp. 75-96. [10.1007/s10652-017-9515-2]

Availability:
This version is available at http://hdl.handle.net/11589/95949 since: 2021-04-08

Published version
DOI:10.1007/s10652-017-9515-2

Publisher:

Terms of use:

(Article begins on next page)

17 November 2026

Vertical dense jet in flowing current

M. Ben Meftah[1], D. Malcangio[1], F. De Serio[1], M. Mossa[1]

[1]Department of Civil, Environmental, Building Engineering and Chemistry, Technical University of Bari, Via E. Orabona 4, 70125 Bari, Italy: e-mail mouldi.benmeftah@poliba.it, daniela.malcangio@poliba.it, francesca.deserio@poliba.it, michele.mossa@poliba.it.

Abstract

The discharge of brackish water, as a dense jet in a natural water body, by the osmotic power plants, undergoes complex mixing processes and has significant environmental impacts. This paper focuses on the mixing processes that develop when a dense round jet outfall perpendicularly enters a shallow flowing current. Extensive experimental measurements of both the salinity and the velocity flow fields were conducted to investigate the hydrodynamic jet behavior within the ambient current. Experiments were carried out in a closed circuit flume at the Coastal Engineering Laboratory (LIC) of the Technical University of Bari (Italy).

The salinity concentration and velocity fields were analyzed, providing a more thorough knowledge about the main features of the jet behavior within the ambient flow, such as the jet penetration, spreading, dilution, terminal rise height and its impact point with the flume lower boundary. In this study, special attention is given to understand and confirm the conjecture, not yet experimentally demonstrated, of the development and orientation of the jet vortex structures. Results show that the dense jet is almost characterized by two distinct phases: a rapid ascent phase and a gradually descent phase. The measured flow velocity fields definitely confirm the formation of the counter-rotating vortices pair, within the jet cross-section, during both the ascent and descent phases. Nevertheless, the experimental results show that the counter-rotating vortices pair of both phases (ascent and descent) are of opposite rotational direction.

Keywords: Dense jet, Shallow flow, Salinity, Velocity, Penetration, Dilution, Vortices.

1. Introduction

The aquatic environment has been always the ultimate sink of wastewater coming from the land. The structure, biodiversity, productivity and functionality of aquatic ecosystems are very sensitive to any water quality changes. The discharge of effluents in a receiving water body via single jet or multiport diffuser, buoyant or non-buoyant jets, reflect a number of complex phenomena [1-9]. Discharge systems need to be designed to minimize environmental impacts. Therefore, a good knowledge of the interaction between the effluents, the discharge system and the receiving environments is required in order to evaluate the mixing process and then the potential environmental impacts. Since many countries around the world suffer water shortages, seawater desalination has become an important alternative source of potable water. Consequently, the amount of brackish water discharged into the aquatic environment by the osmotic power plants is significantly high, making notable effects on the environment.

Over the last decades, research in the field of renewable energy has received a large attention, because of the continuous oil crises and an increasing awareness of the harmful effects of fossil fuels on climate change. Brackish water discharges can be an important energy source, taking advantage of the osmotic pressure due to the mixing of waters of different salinities. This well-known natural phenomenon, the osmosis, allows to transform the chemical energy in mechanical energy and then in electric energy. Since this research is still in its early stage, research activities have until now focused primarily on issues related to plant efficiency [10] as well as on the optimization of the technology to be applied for the use of the membranes [11]. Much less attention

[12, 13] has been paid so far to the analysis of environmental impacts related to the installation of PRO (Pressure Retarded Osmosis) technologies on natural water systems (i. e. rivers, aquifers, sea), taking into account that every manufacturing process entails the production of waste materials, that therefore can be hazardous to aquatic organisms.

Different flow characteristics of this kind of discharge are due to the density differences between the effluent and the receiving water. When the waste water density is higher than the receiving water density, the dense effluent flow tends to fall as negatively buoyant plume. In the contrary case, the effluent is characterized by a neutral to positive buoyant flux causing the plume to rise. The active forces which drive the jet to rise through the overlying water body are the momentum flux at the outlet, and the buoyancy flux due to the difference of density between the effluent and the aquatic ambient. In its permanently delayed movement, the background water is entrained into the jet, expanding it. This process is known as entrainment, which is defined by Pedersen [14] as the diffusion of a fluid characterized by a field of turbulent flow within an environmental fluid in non-turbulent flow.

The beneficial effect of currents on the diffusion of discharges within the water bodies is well known in the literature [15]. A thorough and meticulous discussion on the behavior of vertical, negatively buoyant jets and the several flow configurations that occur at different current speed is presented by Gungor and Roberts [7]. Gungor and Roberts [7] used a laser-induced fluorescence (LIF) technique to measure and map the complete three-dimensional tracer concentration, and therefore dilution, of jets in crossflow at various speeds. Lai and Lee [16] also reported laser-induced fluorescence (LIF) experiments on 60° dense jets discharged into a perpendicular crossflow, then interpreted by a Lagrangian model. Confirming the results of Gungor and Roberts [7], they found that the mixing behavior is governed by a crossflow Froude number u_rF, with u_r is the ratio of ambient to jet velocity, and F is the jet densimetric Froude number. For $u_rF<0.8$, the mixing is jet-dominated and governed by shear entrainment, while when $u_rF\geq0.8$, the dense jet is crossflow-dominated and becomes significantly deflected during its ascent phase. For $u_rF\geq2$, the detrainment ceases to have any effect on the jet behavior [16]. More recently, the study of an inclined (60° to horizontal) dense jet discharged into a cross current in the intermediate field is taken up in the work of Choi et al. [17], whose experimental and numerical results, among others, led to laws that relate the minimum impact dilution to u_rF. Specifically, they found that the minimum dilution varies with $(u_rF)^{1/2}$ in the crossflow-dominated regime, according to Roberts and Toms [4] and Gungor and Roberts [7] for the vertical jet, distinctly different from the $(u_rF)^{1/3}$ dependence as reported by Tong and Stolzenbach [2] and Montessori et al. [13].

Wang et al. [18] numerically investigated the formation processes and vortex dynamics of negatively buoyant starting jets using LES. A revised, directional form of Richardson number (Ri_d) is proposed in [18] to accommodate the entire range of buoyancy, with $Ri_d>0$ for positively buoyant jets, $Ri_d=0$ for non-buoyant jets, and $Ri_d<0$ for negatively buoyant jets. They identified the range Ri_d over which the pinch-off and formation number of starting buoyant jets occurs, extending the buoyant formation model in Wang et al. [19] to negatively buoyant jets.

Among the important physical phenomena associated with a jet in crossflow, there is the formation and evolution of vortical structures within the flow field, in particular the counter-rotating vortices pair (CVP) associated with the jet cross-section. These vortical structures strongly affect the jet behavior, enhancing overall mixing efficiency. Despite the several studies conducted on the understanding of the jet vortical structures in a crossflow, their generation and evolution are still misunderstood, constituting a challenge for any numerical simulation. Gungor and Roberts [7] observed that, with $u_rF=0.9$, at a certain downstream position along the descending region the jet develops a kidney shape characteristic of two counter-rotating vortices. The development of the counter-rotating vortices divides the jet into two almost completely separated halves, leading to strong bifurcation of the jet flow after impacting the bottom. Such a behavior of the jet produces complex flow hydrodynamic structures within the receptor flow body, affecting the mixing process.

Gungor and Roberts [7] also indicated that the rotational direction of these vortices would be opposite to those expected in the ascending flow, but this was not confirmed in their study.

To examine the characteristic properties of a negatively buoyant jet in flowing current, i.e., its penetration within the surrounding ambient, its spreading and its dilution, the present study specifically focuses on the development of the jet vortical structure, based on the flow velocity measurement. Particular attention is paid to the counter-rotating vortices pair evolution and to their rotational direction in both the ascending and the descending phases.

2. Theoretical analysis

According to previous studies on upward dense jet discharged into a crossflow [20-22], it was observed that the jet is almost characterized by two distinct phases: i) a rapid ascent phase, and ii) a gradually descent phase. During the ascent phase, the jet behaves as a vertical pure jet discharged into a crossflow. With a small ratio of the ambient to the jet velocities u_r, the jet is only weakly affected near the exit and vertically penetrates into the crossflow before bending over. In this phase, due to the great effect of its initial momentum, the jet reaches a terminal rise height z_{tm} at a downstream distance x_t from the jet nozzle. During the descent phase, the jet changes to a negatively buoyant plume, where its velocity significantly reduces and the downward buoyant forces cause the discharge to gradually fall back reaching the channel bottom. Near the bottom, the discharge spreads laterally in all directions, forming a bottom layer of spreading density current of thickness z_L. Abessi and Roberts [21] indicated that the rise height could be limited by the ambient depth, H, for shallow water. If the jet reaches the channel surface, its behavior changes, but, due to its negative buoyancy, it eventually detaches from the surface and its centerline impacts the bottom at a downstream distance x_i.

The initial source characteristics (e.g., nozzle shape, dimensions, submerged port height) determine the behavior of the jet discharge in the near field region. The initial momentum flux, the buoyancy flux, and the discharge angle determine the jet penetration and mixing level within the ambient flow. The hydrodynamic features of the cross current (e.g., depth, flow rate, stratification, wave motion) can have a significant influence on the mixing in the near field region, but its presence enhances more the discharge dilution. Fig. 1 shows a definition sketch of a typical dense jet discharged normally into a main shallow flow. The jet consists of a vertical round nozzle with an inclination angle relative to the horizontal θ=90°, a diameter D and a port height z_0, which releases the effluent with an initial density ρ_0 into a channel crossflow of fluid density ρ_a, with $\rho_a<\rho_0$. In the present study, the effluent consists of saline water solution of initial conductivity c_0, while that of the ambient receptor is c_a ($c_a<c_0$). The jet discharges at an initial velocity U_0, whereas the uniform channel/ambient flow has a mean velocity U_a. Fig. 1 also shows the jet centerline trajectory, determined as the locus of the maximum salinity concentrations (maximum conductivity). At the downstream distance x_t, the minimum dilution through the jet cross-section at the terminal rise height, which coincides with the centerline trajectory at a rise height z_t, is defined as s_t. The minimum dilutions at the impact point, at a downstream position x_i, is defined as s_i. All the basic symbols and the system of coordinates are clearly indicated in Fig. 1.

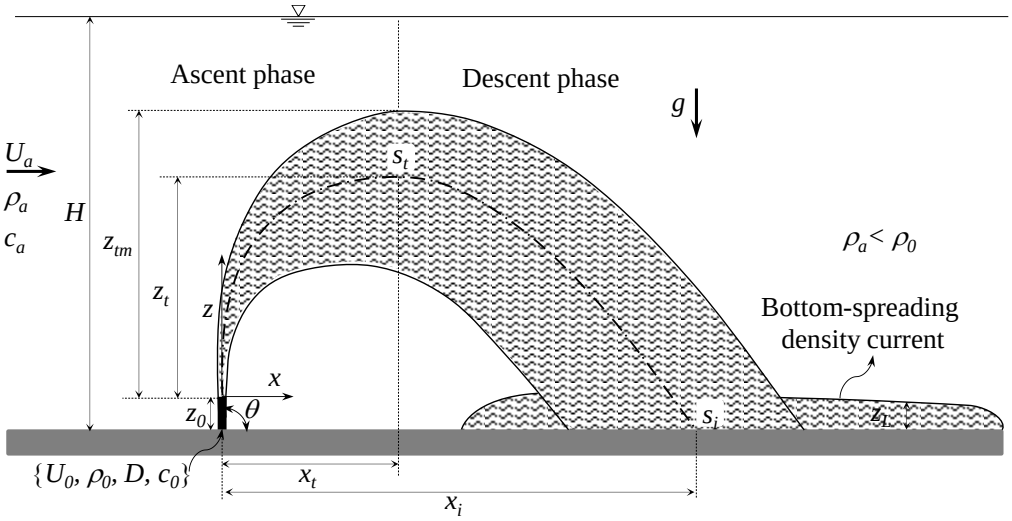


Fig. 1 Definition sketch of vertical dense jet in shallow water.

Many investigators [1, 4, 7] have analyzed inclined dense jet discharged into a crossflow. They characterized the discharge by the source fluxes, that is, the discharge volume flux Q_0, the momentum flux M_0 and the buoyancy flux B_0, defined as:

$$\begin{aligned} &Q_0 = U_0 A_0; \qquad M_0 = Q_0 U_0; \qquad B_0 = g' Q_0 \\ &A_0 = \frac{\pi}{4} D^2 \end{aligned} \tag{1}$$

where A_0 is the jet source area (initial discharge cross-sectional area), $g' = [(\rho_0 - \rho_a)/\rho_a]g$ is the initial reduced gravity and g is the gravity acceleration. These fluxes can be combined with the ambient velocity, U_a, to provide some relevant length scales, such as:

$$l_M = \frac{M_0^{3/4}}{B_0^{1/2}}; \qquad l_m = \frac{M_0^{1/2}}{U_a}; \qquad l_Q = \frac{Q_0}{M_0^{1/2}}; \qquad l_B = \frac{B_0}{U_a^3} \tag{2}$$

The significance of these scales and their ratios is discussed in several previous studies [1, 4, 7, 23, 24]. Briefly, l_M is the jet-to-plume length and measures the relative importance of the initial momentum and buoyancy fluxes, differentiating the region of the jet-like mixing dominance from the region of buoyancy dominance, l_m is the jet-to-crossflow length scale and measures the relative importance of the initial jet momentum to the ambient flow velocity, l_Q is the discharge length scale and indicates the distance over which the volume flux of the entrained ambient fluid becomes approximately equal to the initial volume flux, l_B is the plume-to-crossflow length scale and represents the vertical location where the plunging plume becomes strongly influenced by the ambient flow. According to Roberts and Toms [4] and to Gungor and Roberts [7], a velocity scale can also be provided as:

$$U_c = \frac{B_0^{1/2}}{M_0^{1/4}} \tag{3}$$

Since any dependent variable denoted by Φ can be characterized as a function of the jet and ambient variables as:

$$\Phi = f\left(Q_0, B_0, M_0, U_a, \theta, H, B\right) \tag{4}$$

any dimensionless jet property Φ' can be expressed as:

$$\Phi' = f\left(\frac{l_Q}{l_M}, \frac{U_a}{U_c}, \theta, \frac{B}{H}\right) \tag{5}$$

For vertical jets, θ is invariant. For shallow flow, the mean flow depth, H, is much smaller than the mean channel width, B, that is $H/B<<1$ (in the present study $H/B=0.09$ for all experimental runs), thus Eq.(5) becomes:

$$\Phi' = f\left(\frac{l_Q}{l_M}, \frac{U_a}{U_c}\right) \tag{6}$$

The ratio l_M/l_Q in Eq.(6) is proportional to the jet densimetric Froude Number F

$$\frac{l_Q}{l_M} = \left(\frac{\pi}{4}\right)^{1/4} \left(\frac{U_0}{(Dg')^{1/2}}\right)^{-1} = \left(\frac{\pi}{4}\right)^{1/4} F^{-1} \tag{7}$$

According to Gungor and Roberts [7], the dynamical effect of the ambient current is mainly determined by the ratio of the ambient velocity to the characteristic velocity U_a/U_c, which is also equal to l_M/ l_m. For round jet nozzle this ratio can be expressed as:

$$\frac{U_a}{U_c} = \left(\frac{\pi}{4}\right)^{-1/4} u_r F \tag{8}$$

Eqs. (6-8) clearly indicate that all the dependent geometric scales of the flow, such as x_t, x_i, z_t, z_{tm} can therefore be written as:

$$\frac{x_t}{DF}, \quad \frac{x_i}{DF}, \quad \frac{z_t}{DF}, \quad \frac{z_{tm}}{DF} = f\left(F,\ u_r F\right) \tag{9}$$

taking into account that l_M is proportional to DF.

The jet dilution is related to the density variation in the flow field. The local modified acceleration due to gravity $g''=g\,[(\rho-\rho_a)/\rho_a]$ can be taken as a jet dependent property, where ρ is a local fluid density. Following a dimensional analysis used by Roberts and Toms [4], based on the length scale l_M and the velocity scale U_c, the dilution $S=g'/g''=[(\rho_0-\rho_a)/(\rho-\rho_a)]$ can be determined as:

$$S\frac{l_Q}{l_M} = \frac{S}{F} = f\left(F,\ u_r F\right) \tag{10}$$

Roberts and Toms [4] and Gungor and Roberts [7] observed that, for $l_Q<<l_M$ ($F>>1$), the dynamic effect of the source volume flux becomes negligible, and thus F does not appear as an individual variable. After these assumptions, Eq. (9) becomes:

$$\frac{x_t}{DF},\quad \frac{x_i}{DF},\quad \frac{z_t}{DF},\quad \frac{z_{tm}}{DF},\quad \frac{S_t}{F},\quad \frac{S_i}{F} = f\left(u_r F\right) \tag{11}$$

3. Experimental method

Experiments were carried out in a closed circuit laboratory flume expressly designed for buoyant jets study at the Laboratory of Coastal Engineering (LIC) of the Department of Civil, Environmental, Building Engineering and Chemistry, Technical University of Bari (Italy). The system consists of a rectangular channel, 15m long, 4m wide and 0.4m deep (Fig. 2). The experimental walls of the flume are made of transparent glass panels 0.015m thick and supported by a steel frame. The fresh water at ambient temperature is supplied from a downstream large metallic tank by a Flygt centrifugal electro-pump, and then discharged through a steel pipe with 0.2m diameter into the upstream steel tank, with a side-channel spillway with adjustable height in order to maintain a constant and uniform water head. The overflowing water is directed into a parallel pipe with 0.2m diameter and finally discharged into the storage tank downstream of the channel. Two electromagnetic flow meters are mounted on the two parallel pipes described above in order to measure the flow rate in the channel as the difference between the two discharge measurements.

The second part of the laboratory model consists of a dense jet hydraulic system. For the fresh water supply and its salination, a circular storage tank made by fiberglass is used, with maximum volume of 6000l, which is able to supply four consecutive steady-dense jet configurations avoiding salinity variations in the current higher than 10%, considering the closed hydraulic circuit of the flume. The tank is equipped with four compressed air jets diametrically opposed inside to mix the water up to the fixed salinity, and a conductivity/temperature probe to measure the initial jet salinity. Table salt (NaCl) is added to the fresh tap water as the source of negative buoyancy, maintaining a constant conductivity for each runs [30 and 28 mS/cm for run R1 and runs R2-R4, respectively]. The salty water is pumped, through a magnetic flow meter, to the jet nozzle of diameter D=10mm, vertically mounted at the center of the flume with a port height z_0=10mm from the bottom boundary.

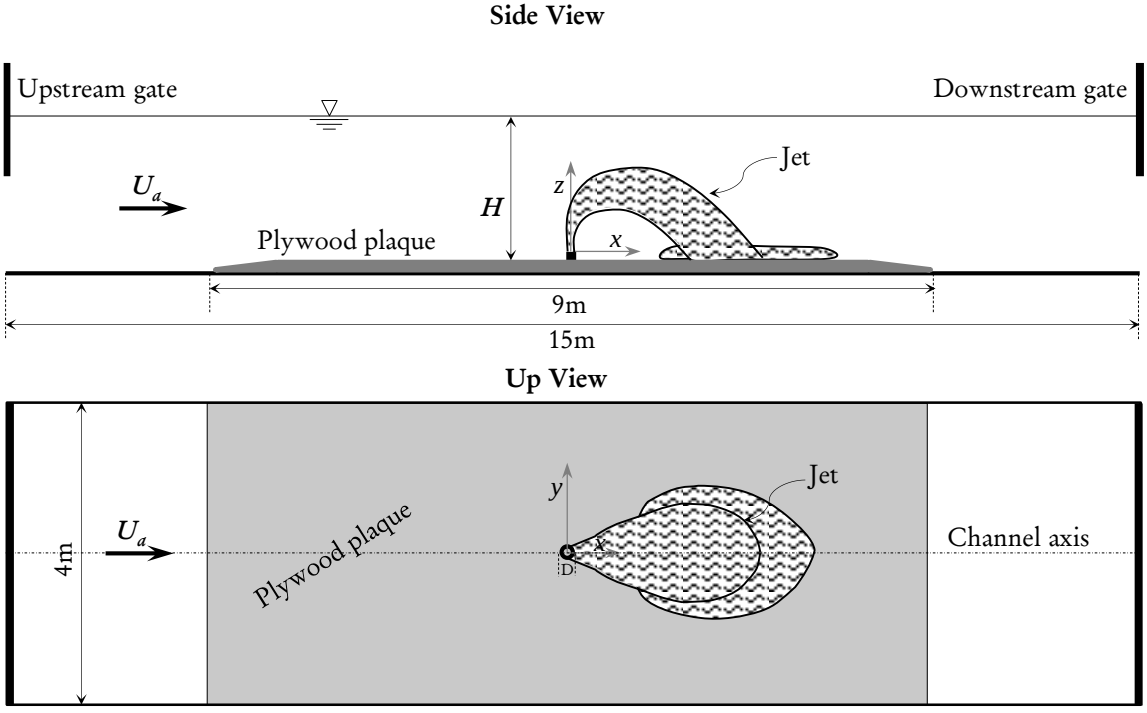


Fig. 2 General sketch of the laboratory flume with the jet flow.

The study of the dense jet dilution in the crossflow is performed by means of punctual measurements of salinity and velocity fields. The flume is equipped with a sliding support for measurement instruments, which enables the latter to be displaced along the three spatial directions (longitudinal *x*, transversal *y* and vertical *z*), and to collect data at several longitudinal and transversal sections. The salinity field was measured by means of a Micro Scale Conductivity Temperature Instrument (MSCTI) by Precision Measurement Engineering (PME), designed to measure the temperature and electrical conductivity of water solutions and moving fluids containing conductive ions. Before each test, the probe was calibrated by a solution prepared in laboratory. At each measurement location, 1000 conductivity data were collected at 20Hz. The linear conductivity ranged from 0.05S/m to 80S/m while the temperature from 0°C to 40°C, and the output voltage range was ±5 V. The velocity data were collected using 3-D Acoustic Doppler Velocimeter (ADV)-Vectrino system, developed by Nortek, for 60sec at a sampling rate 150Hz. The sampling volume of ADV was located 5cm below the transmitter probe. The Vectrino was used with a velocity range equal to ±0.30m/s, a measured velocity accuracy of ±0.5%, a sampling volume of vertical extent of 7mm. For high-resolution measurements, the manufacturer recommends a 15db signal-to-noise ratio (SNR) and a correlation coefficient larger than 70%. The acquired data were filtered based on the Tukey's method and the bad samples (SNR<15db and correlation coefficient <70%) were also removed. Additional details concerning the channel setup and the ADV operations can be found elsewhere in [25-31].

The initial experimental conditions and some parameters of the performed experimental runs are reported in Table 1, where $Re_0=U_0D/\nu_0$ is the initial jet Reynolds number and ν_0 is the initial kinematic viscosity of the jet. In addition to the experimental data of the present study, in Table 1 we also illustrate the data obtained by Gungor and Roberts [7] for ten configurations with different values of u_rF.

Table 1 Initial experimental conditions and parameters of the investigated runs. NI stands for not identified

	Runs	U_0 (m/s)	Re_0 (-)	F (-)	u_rF (-)	s_t/F (-)	s_i/F (-)	$z_{tm}/(DF)$ (-)	$x_i/(DF)$ (-)
Present study	**R1**	0.32	2769	7.7	1.0	1.084	2.60	1.69	4.16
	R2	0.38	3340	9.8	1.1	1.131	2.91	1.73	4.07
	R3	0.45	3719	11.4	1.1	NI	NI	1.84*	4.3*
	R4	0.51	4250	13.1	1.1	NI	NI	1.87*	4.3*
Gungor and Roberts [7]	**DJV01**	NI	NI	20.9	0.522	0.593	1.54	2.96	2.87
	DJV02	NI	NI	20.1	0.511	0.790	1.63	2.89	3.01
	DJV03	NI	NI	20.7	0.915	0.997	2.31	2.47	6.12
	DJV04	NI	NI	23.0	0.233	0.421	1.67	2.76	1.16
	DJV05	NI	NI	22.5	0.232	0.541	1.99	2.79	1.49
	DJV06	NI	NI	19.0	0.692	0.952	2.33	2.80	5.24
	DJV07	NI	NI	23.7	0.243	0.389	1.24	2.49	1.36
	DJV08	NI	NI	21.6	0.373	0.477	1.23	2.96	-
	DJV09	NI	NI	21.5	0.220	0.351	1.41	2.96	1.32
	DJV10	NI	NI	20.9	0.213	0.432	2.03	2.93	0.75

*Values estimated based on the velocity trajectories

4. Results and discussion

4. 1. Jet dilution

Figs. 3a-b) show maps of the jet dilution in the surrounding flow environment. The data refer to runs R1 and R2 characterized by a velocity ratio u_r equal to 0.131 and 0.109, respectively. The dimensionless jet excess salinity (conductivity) is determined on the basis of the mean values of the measured conductivity field as:

$$C = \frac{c - c_a}{c_0 - c_a} \tag{12}$$

where c is the local time-averaged conductivity, c_a is the conductivity of the ambient flow and c_0 is the conductivity of the initial discharged effluent. The jet dilution is simply defined as $s=1/C$. The effluent concentration within the mixing zone rapidly reduces as going further downstream of the jet source, reaching the ambient flow values. Therefore, in the present study the field conductivity c was intensively measured in the plane of flow symmetry (y=0) of both the dense jet and the channel flow.

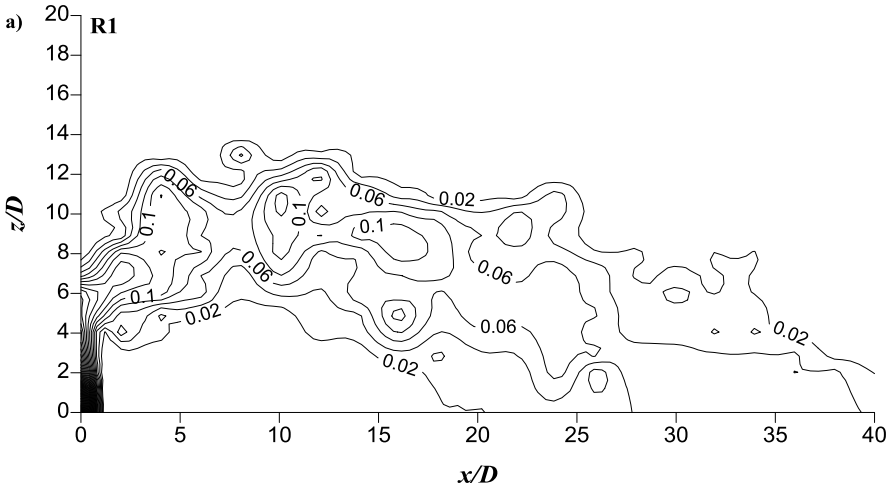
In Figs. 3a-b), the contour line intervals of the dimensionless excess jet salinity have constant spacing of 0.02. In order to clearly represent the jet trend within the surrounding ambient flow, the salinity values smaller than 0.02 (2%) are not plotted in Figs. 3a-b). Theoretically, the salinity outside the mixing zone, i.e., in the pure ambient flow, is reduced to nil, which is difficult to reach experimentally. For this reason, in Figs. 3a-b) only salinity values greater than 2% were plotted, to distinguish the jet region from the ambient flow domain. As a result, Figs. 3a-b) clearly show the jet penetration within the ambient flow. It can be clearly noted that the dense jet is divided into two distinct regions/phases:

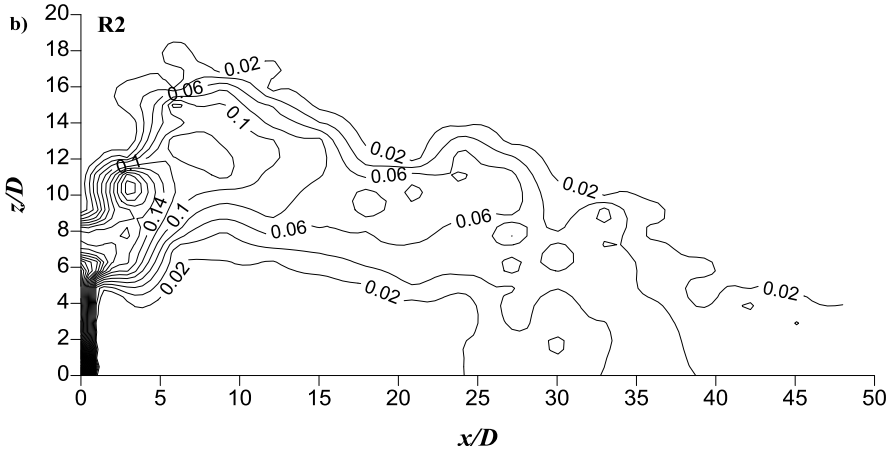
i) the first region, starting from the jet nozzle position, in which the jet undergoes rapid ascent toward the channel free surface flow, reaching its maximum rise height. In this region, the jet behaves almost like a vertical pure jet discharged into a crossflow [3, 8]. Close to the nozzle, the jet undergoes an almost vertical ascending portion of order 2D to 4D for runs R1 and R2, respectively. In this portion the jet width is O(1D) and the salinity concentration C shows maximum values nearly equal to 1 (100%). This implies that, analogously to pure jets, nearby the jet nozzle a kind of potential jet core takes place, where the initial effluent concentration remains almost invariant. The length of the jet core is inversely proportional to the velocity ratio u_r, in fact it increases as u_r decreases. From the end of the potential jet core, the jet starts to bend over by the ambient cross-flow along the downstream distance x_t (see Fig. 1). At x_t, Figs. 3a-b) indicate that the jet becomes almost horizontal, and then begins to descend;
ii) the second region is a descent region, starting from the downstream distance x_t where the jet reaches its maximum height, and develops till the impact point of the jet at the channel bottom. Figs. 3a-b) clearly show that the descent region extends longer downstream than the ascent region, which is in good agreement with observations in previous studies [4, 7, 21, 31]. In contrast to the ascent phase, where the jet rapidly penetrates within the ambient flow due to the effect of high momentum, during the descent phase the jet gradually descends under the buoyancy effects. The substantial expansion of the jet and its entrainment with the surrounding ambient flow, during the descending phase, lead to a significant reduction of the jet momentum. The decrease of the jet momentum, in addition to the ambient current speed U_a, strongly affects the downstream extending of the descent region.

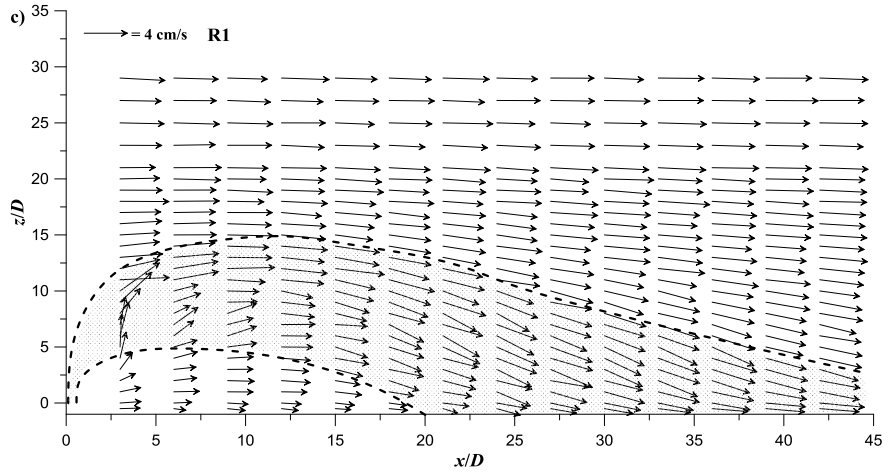
Figs. 3a-b) show that the jet penetration height within the ambient flow and the whole downstream jet spreading (of both the ascent and descent regions) significantly change from run R1 to run R2. In run R1, the jet almost attains a terminal rise height z_{tm} of an order 14D over a downstream distance x_t = 9D and develops further downstream, touching the channel bottom over a width almost ranging between x=20D to 40D. Whereas, run R2 almost experiences a z_{tm} of order 18D, a x_t of order 11D and an impacting area of the jet on the channel bottom almost covering a distance from x=25D to 50D. Figs. 3a-b) point out that the jet of run R2 penetrates deeper into the crossflow and gradually bends over as going further downstream, allowing a greater extension of the jet within the surrounding flow before impacting the channel bottom. Figs. 3a-b) also show that the vertical width (between the upper and lower limits of the jet) increases with decreasing u_r.

Figs. 3c-f) shows vector maps of the resultant flow velocity (sum of the streamwise U and vertical W, time-average velocity components) in the plane of flow symmetry (y=0) of runs R1 to R4, obtained using the Acoustic Doppler Velocimeter (Vectrino). In Figs. 3c-f) the outer and inner boundaries of the jet were qualitatively plotted, as shown by the dashed lines. The area of the jet flow enveloped by its boundaries is indicated by the gray dotted-area. Confirming what already noted in Figs. 3a-b), also Figs. 3c-f) clearly show the jet penetration within the ambient flow. Nearby the jet nozzle, at x/D=3, the vector velocities within the jet flow, especially in its central region, appear almost vertical, while they slightly bend over approaching the outer boundary of the jet. This is more pronounced as F increases, i.e., in runs R3 and R4. As going further downstream, the jet is more deflected toward the horizontal. Figs. 3d-f) clearly indicate that the downstream position of the jet terminal rise height is significantly dependent on F, i.e. it increases as F increases. For run R1, at x/D=9, the velocity vectors seem to be almost horizontal, indicating that the jet reaches its terminal rise height; instead for R4, it happens further downstream of x/D=12. The flow velocity fields of runs R1 to R4 show that this behavior is accompanied by an increase of the jet penetration height within the ambient flow, as F increases. Moreover, the area of the jet flow becomes larger with the growth of F. After reaching its terminal rise height, the jet undergoes a gradual downward curvature until impacting the channel bottom. Figs. 3c-f) suggest that the curving degree of the jet, during the descending phase, appears less steep with the largest values of F, allowing the jet to penetrate further downstream before touching the channel bottom. At x/D>35, Fig. 3c) shows an almost horizontal spreading of the jet in the direction of the mean flow. This should indicate the beginning of the bottom-spreading density current, as also noted in Figs. 1 and 2.

As previously written, Gungor and Roberts [7] carried out detailed measurement of the tracer concentration of turbulent vertical dense jets discharged in flowing currents using a three-dimensional laser-induced fluorescence technique. This technique enables accurate measurement of the jet concentrations, giving more details on the jet behavior than a point-probe method, as used in the current study. Despite the difference between both techniques, the results obtained by Gungor and Roberts [7] for their experiment with u_rF=0.9 show the same behavior of the jet within the ambient flow as shown in Figs. 3a-b). It should be noted that run R1 and R2 were carried out with a current speed u_rF=1.01 and 1.07, respectively (Table 1). Figs. 3a-b) clearly show a kind of vertical asymmetry, referring to the location of minimum dilution (maximum concentration). This asymmetry between the upper half of the jet (above the minimum dilution) and the lower half (below the minimum dilution) is more pronounced in the ascending phase. With the descending phase this asymmetry is less pronounced and seems to vanish as going further downstream. The experimental results of Gungor and Roberts [7] with u_rF=0.9, confirm this assessment. The authors [7] observed that a slight asymmetry occurs in the ascending portion, but in the descending phase, the vertical profiles of the jet dilution almost show vertical symmetry. Moreover, Gungor and Roberts [7] observed that through a three-dimensional representation of the dense jet, at a certain downstream position with the descending region, the jet develops a kidney shape characteristic of two counter-rotating vortices. The authors [7] found that the development of the counter-rotating vortices divides the jet into two almost completely separated halves, leading to strong bifurcation of the jet flow after impacting the bottom. Such a behavior of the jet produces complex flow hydrodynamic structures within the receptor flow body, which makes a numerical prediction of these flows quite challenging.


a)
R1
z/D
x/D
0.1
0.06
0.02


b)
R2
z/D
x/D
0.1
0.06
0.02


c)
= 4 cm/s
R1
z/D
x/D

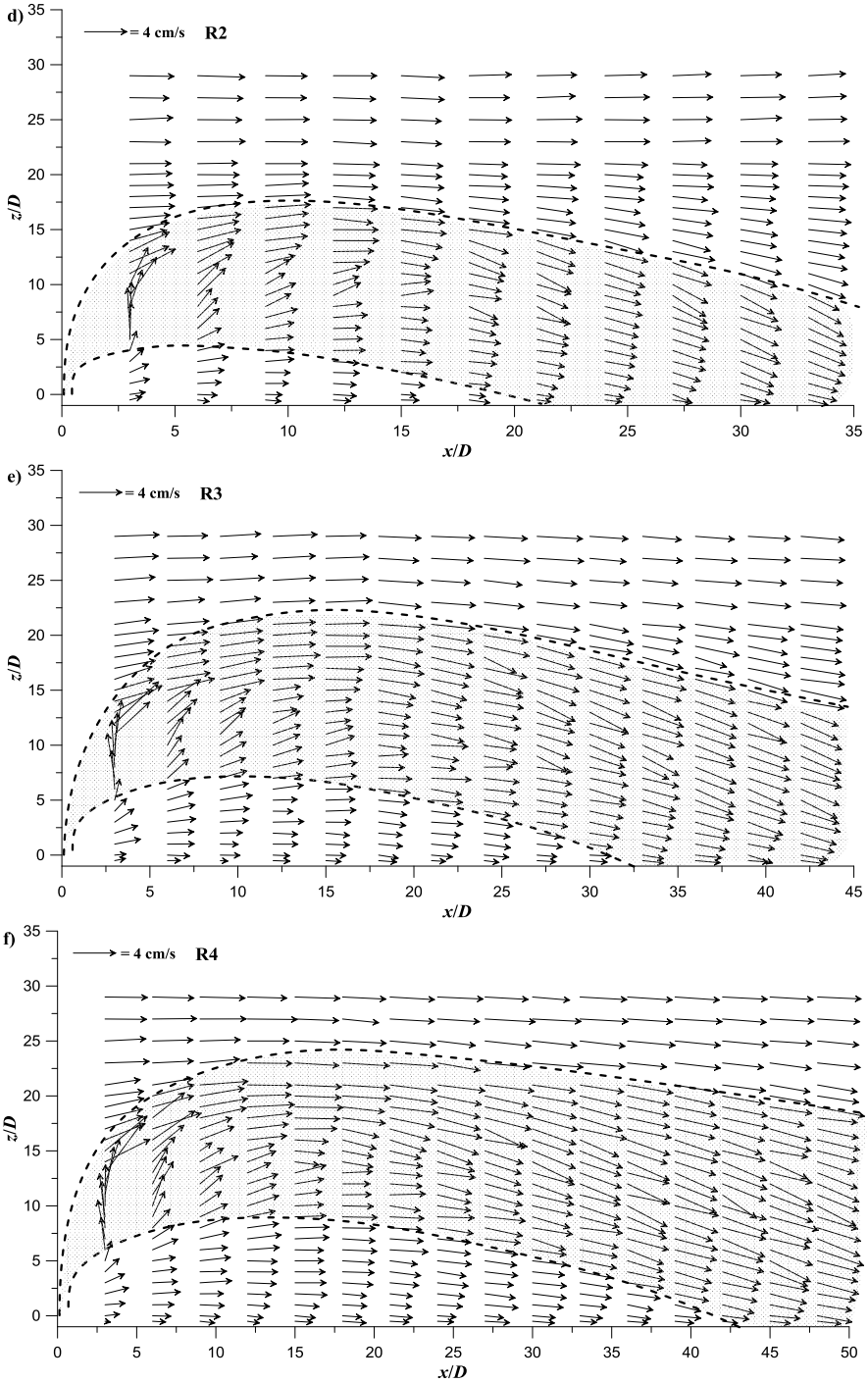


Fig. 3 Jet penetration within the ambient flow (along the plane of the jet flow symmetry), a-b) map of the jet salinity *C*-distribution for runs R1 and R2, c-f) vector maps of the resultant velocity field for Runs R1 to R4.

Figs. 4a-h) depict the vertical profiles of the distribution of the dimensionless excess jet salinity *C*, at different downstream positions *x*/*D* = 6, 10, 18 and 30 for run R1 and *x*/*D*= 6, 12, 18 and 36 for run R2. All the profiles clearly indicate the increase of *C* within the jet flow. Outside the jet flow, *C* always remains constant along the vertical, with zero values. This region indicates the pure ambient flow (without discharged effluents). It is worth mentioning that in this study extensive measurements of the salinity vertical profiles, similar to those illustrated in Fig. 4, were carried out with a downstream displacement step-length of 2D for run R1 and 3D for run R2, and with a vertical displacement step-length of 1D for both runs. These profiles are known to be useful for determining all the jet properties, i.e., its upper and down limits, its vertical width and its centerline trajectory, based on the maximum values of *C*.

Fig. 4 clearly shows an asymmetry of the vertical profile, as previously discussed, with the ascending phase. This is well pronounced in Figs. 4a) and e) at x/D=6 for both runs R1 and R2. At the downstream position x/D=10 and 12 [Figs. 4b) and f)] for run R1 and R2, respectively, the asymmetry between the upper and lower halves of the jet is less pronounced than at x/D=6. It is to be noted that the downstream positions at x/D=10 and 12 are very close to the position of the terminal rise height, x_t, of the jet for both runs. Further downstream, in the descending region, the jet has an almost symmetric vertical distribution between its upper and lower halves. This is well pronounced at the downstream position x/D=18 for both runs [Figs. 4c) and g)]. At x/D=30 and 36 respectively for runs R1 and R2, the peaks of the salinity profiles take place at the level of the channel bottom [Figs. 4d) and h)], showing only the upper jet half. This experimental result implies that these positions are very close to the jet centerline impact point x_i, as shown in Fig. 1. Gungor and Roberts [7] observed that at low speeds (u_rF<0.5), the descending flow is strongly asymmetric, due to a kind of gravitational instability that can cause detrainment of fluid from the plume into the rising jet, creating very complex hydrodynamic structures. Moreover, the authors [7] noted that, with low current speeds, the jet undergoes a sharp curvature at its terminal rise height, causing centrifugal forces.

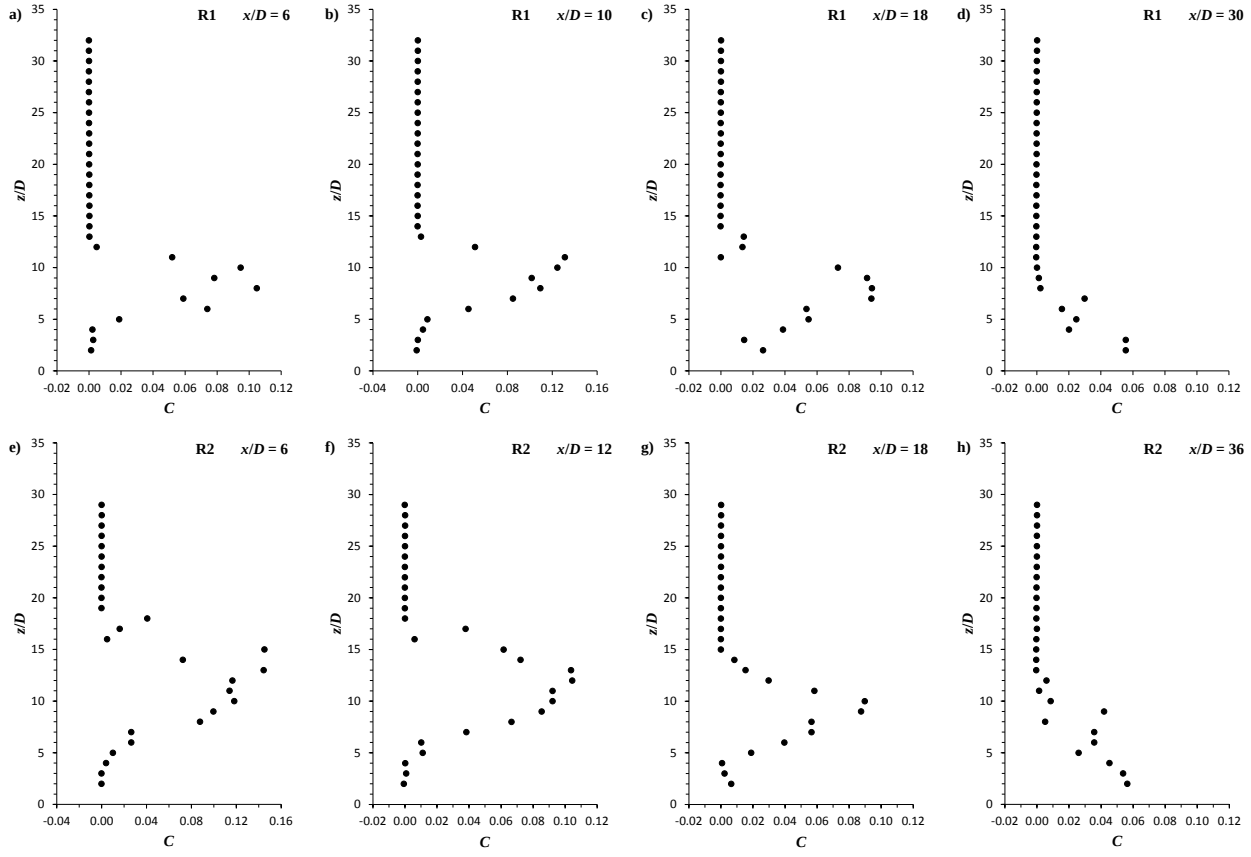


Fig. 4 Vertical profiles of the jet salinity C at different downstream positions for runs R1 (above) and R2 (below).

Moreover, Fig. 4 highlights that, for both runs R1 and R2, the jet undergoes a strong dilution during the initial rising phase, along a downstream distance of order almost 6D. Along this rising portion, the jet salinity C, for both runs, is approximately reduced by more than 85%, compared to its initial salinity C_0=100%. From x/D=6, the jet salinity continues to decrease (i.e. dilution continues to increase) in a very gradual manner as going further downstream. From x/D=6 to x/D=18, the variation of the jet concentration is limited to about 5% for both runs. Finally, the jet impacts the channel bottom with a maximum concentration (at centerline trajectory) lower than 6%, as shown by Figs. 4d) and h) at x/D=30 and 36 for runs R1 and R2, respectively.

Gungor and Roberts [7], in their experiment with u_rF=0.9, obtained a maximum tracer concentration nearby the terminal rise height position (x/DF=1.63 or x/D=33.74) of almost 40% against a value O(12%) obtained for runs R1 and R2 of the current study, as shown in Figs. 4b) and f). In the descending region, Gungor and Roberts [7] found a concentration of order 30% and 20% at the downstream position x/DF=3.09 (x/D=63.96) and 4.55 (x/D=94.18). It follows that the downstream variation of the tracer concentration in the descending region (of order 10% from x/DF=1.63 to x/DF=3.09) obtained by Gungor and Roberts [7] is slightly larger than the variation rate obtained in the present study. However, both jet concentration distributions prove the gradual development of the dense jet during the descending phase. The significant increase of the jet dilution noted in the present study, in comparison with the results of Gungor and Roberts [7], can be explained by the increase in the current speed. Specifically, while Gungor and Roberts [7] conducted their laboratory experiments with a range of the current speed u_rF varying between 0.2 and 0.9, for this study u_rF is equal to 1.01 and 1.07, for runs R1 and R2, respectively. Same authors [7] confirmed that the jet dilution increases as u_rF increases., Moreover, they deduced the following empirical equations, using other data from previous studies, to predict the jet dilution at its terminal rise height and at its impacting point with the channel bottom, respectively, as:

$$\frac{s_t}{F}=0.87\left(u_rF\right)^{1/2} \tag{13}$$

$$\frac{s_i}{F}=2.3\left(u_rF\right)^{1/2} \tag{14}$$

Figs. 5 and 6 show the values of the normalized jet dilution s_t/F, at the terminal rise height, and s_i/F, at the impact point, versus the normalized current speed u_rF, respectively. Figs. 5 and 6 clearly confirm the proportionality of the jet dilution, at both downstream positions x_t and x_i, to the current speed u_rF. Despite the data scattering of s_i/F by Gungor and Roberts [7] at low values of u_rF, in Fig. 6 the jet dilution almost follows the empirical equations (13) and (14).

4. 2. Jet cross-section structure

Since the results of previous experimental studies [4, 7, 21, 32] reveal very complex behavior of the discharge of dense jets in flowing currents, analysis of the jet properties limited to the vertical plane of flow symmetry (y=0) are not enough to understand such a phenomenon. In order to improve knowledge on the jet mixing process within the ambient current, measurements of the jet properties through the transversal cross-sections were also investigated. As an example, Fig. 7 illustrates the dimensionless salinity distribution C through the jet cross-sections of run R1, obtained at the downstream positions x/D=10 and 18. The choice of these downstream positions is due to the fact that: i) around the position x/D=10 the jet almost attains its terminal rise height and therefore its front cross-section becomes completely vertical and normal to the mean ambient current, thus avoiding distorted data of the jet properties; ii) during the descending phase, i.e. around x/D=10, the jet undergoes its most important deformations, such as the development of the counter-rotating vortices pair, as noted in Gungor and Roberts [7]. Since the jet and the channel flows are symmetric with respect to the vertical plane at y=0, in Fig. 7 only the data of the half cross-section are plotted. In Fig. 7 the contour line intervals of the normalized excess salinity concentration have a constant spacing of 0.02, as in Fig. 3.

Fig. 7 shows the lateral dispersion of the jet within the ambient flow. At x/D=10, the maximum values of the salinity concentration take place around the jet centerline trajectory position. As going further away from the jet center, C undergoes a progressive decrease with almost the same rate in all direction, showing a kind of radial symmetric distribution. At this position, the jet shows a "*walnut*" shape rather than the familiar kidney shape, without evidence of the

development of the counter-rotating vortices pair. At *x*/*D*=18, however, the jet cross-section considerably modifies its width increases, showing the familiar kidney shape formation. It is noteworthy that the kidney shape of the jet cross-section is concave upward, which is opposite to the familiar kidney shape obtained with ascending pure jet [3, 8]. Gungor and Roberts [7] observed the same jet behaviors at such a position during the descending phase, confirming the development of counter-rotating vortices pair. They also indicated that the rotational direction of these vortices would be opposite to those expected in the ascending flow, but this was not confirmed in their study.

In order to get more details, Figs. 8a-f) show the field of the resultant velocity distribution (sum of the transversal, *V,* and vertical, *W*, time-average velocity components) through the channel-jet cross-section, at the downstream positions *x*/*D*=10 and 18 for runs R1 to R3. Fig. 8a) shows a kind of random velocity distribution within the jet cross-section, where no clear evidence of the development of the counter-rotating vortices pair is found. However, focusing on the jet flow velocity field in Fig. 8a), the velocity vectors trend shows a clockwise rotation of the flow at this position, as indicated by the curved arrow dashed-line on the figure. The lack of clarity of the development of the counter-rotating vortices pair in Fig. 8a) can be explained by the fact that, at the downstream position x/D=10, the jet in run R1 almost attains its terminal rise height (see Fig. 3c), which is a position of flow transition between the ascending and descending phases. On the contrary, Figs. 8c and e) clearly show an evident development of a clockwise vortex within the jet cross-section. It is worth noting that at the downstream position x/D=10, as shown in Figs. 3d-c), the jet in runs R2 and R3 has not yet reached its terminal rise height, belonging to the ascending phase. Consequently, Figs. 8c and e) also confirm the presence of the counter-rotating vortices pair within the jet cross-section during the ascending phase. This result was not achieved by Gungor and Roberts [7], based only on the flow salinity field measurements. Gungor and Roberts [7], in addition, suggested the non-development of such a structure during the ascending phase, indicating the possibility of its occurrence only during the descending phase. At *x*/*D*=18, Fig. 8b) displays, however, a clear tendency of a counter-clockwise vortex through the jet cross-section. The same tendency is also noted in Figs. 8d and f) at the same downstream position *x*/*D*=18. Since the jet flow is axis-symmetric, this also confirms the development of the counter-rotating vortices pair, within the jet cross-section, during the descending phase. As clearly shown in Figs. 8b, d and f), the jet flow vortices, in the descending region, rotate in an opposite direction compared to those observed in the ascending region (Figs. 3d-c)) and to those expected in ascending jet flows [3, 8]. According to Gungor and Roberts [7], the counter-rotating vortices pair, in the descending region, cause the jet to almost completely bifurcate after impacting the bottom, affecting the mixing process and consequently the jet dilution.

The findings from this study are highly suggestive in regard to the vortical structure developement and its eventual effect on the mixing processes of a vertical dense jet discharged into a flowing current. The experimental results certainly confirm the formation of the counter-rotating vortices pair in the descending region, which was not clear in Gungor and Roberts [7]. Furthermore, the flow velocity fields clearly suggest the development of such a structure, also, during the ascending phase, which was not proved in previous studies [7]. Finally, the present study specifies that the counter-rotating vortices pair of the jet in the ascending and descending regions are of opposite rotational direction.

According to the previous study of Gungor and Roberts [7], the maximum jet rise height and the downstream position of the jet impact point (defined as where the jet centerline intersects with the horizontal plane at the level of the jet nozzle mouth) can be predicted by the following semi-empirical equations:

$$\frac{z_{tm}}{DF} = 2.8 \qquad \text{for} \quad 0.2 < u_r F < 0.8 \tag{15}$$

$$\frac{z_{tm}}{DF}=2.5\left(u_r F\right)^{-1/3} \qquad \text{for} \quad u_r F>0.8 \tag{16}$$

$$\frac{x_i}{DF}=5.6\left(u_r F\right) \tag{17}$$

Figs. 9 and 10 depict the maximum rise height and the downstream position (relative to the jet source position) of the impacting point of the jet, both normalized by the *DF*-product and plotted versus the current speed parameter u_rF. It is worth mentioning that in Figs. 9 and 10 the data of R3 and R4 are estimated based on the velocity trajectories (positions of the maximum values of the jet velocity) and not on the jet centerline (positions of the maximum values of the jet salinity concentration), which are slightly different [3]. Fig. 9 shows that, for u_rF>0.8, Eq. (16) overestimates the jet maximum rise height of the present study compared to that of Gungor and Roberts [7]. Fig. 10 also shows a slight overestimation of the downstream position of the jet impacting point by Eq. (17). This could be due to the measurement uncertainty for both studies in addition to the few data (only two points) used by Gungor and Roberts [7] for u_rF>0.8, which could affect the empirical coefficient of Eq.(16). Anyhow, Figs. 9 and 10 show that all data roughly follow the trend of the proposed semi-empirical equations (15-17), predicting z_{tm} and x_i.

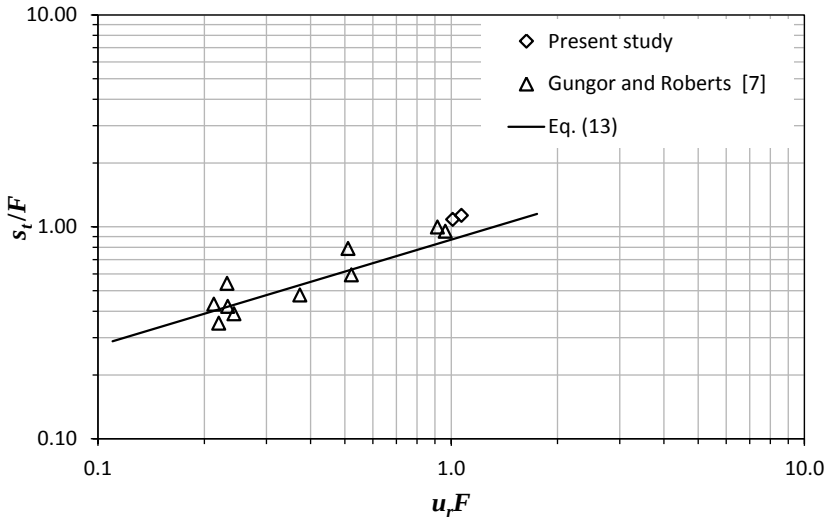


Fig. 5 Dilution at the jet terminal rise height.

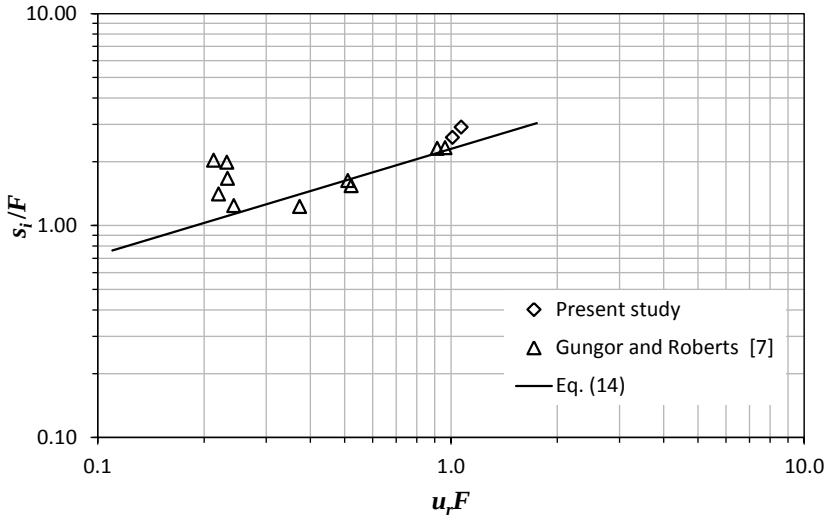


Fig. 6 Dilution at the jet impact point.

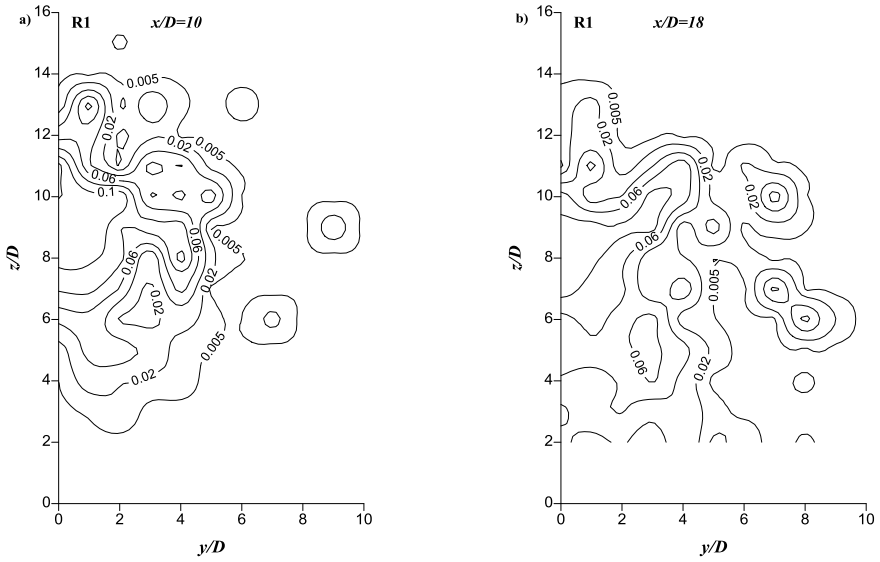
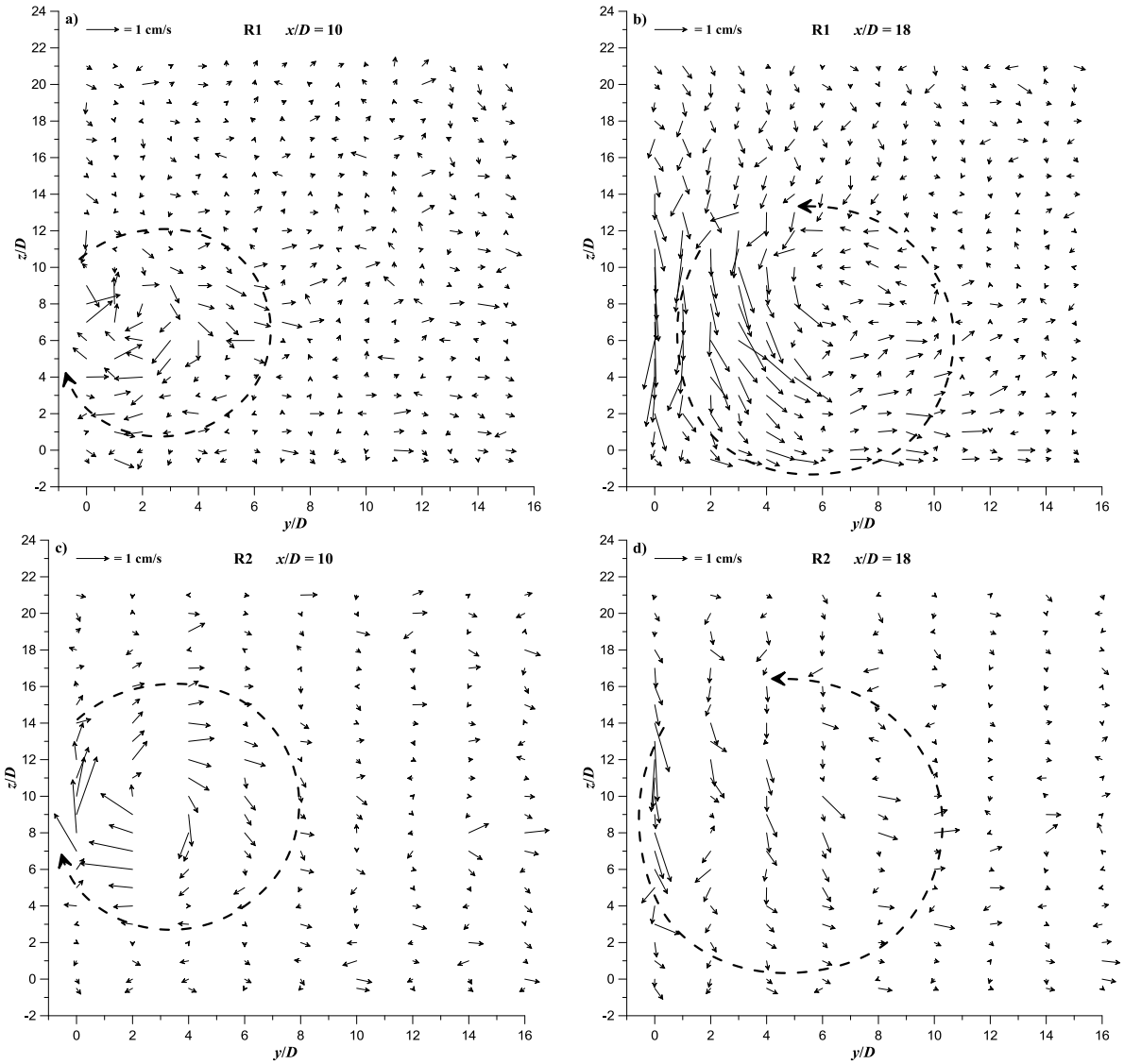


Fig. 7 Contour plot of the jet salinity *C* through the jet cross-sections.



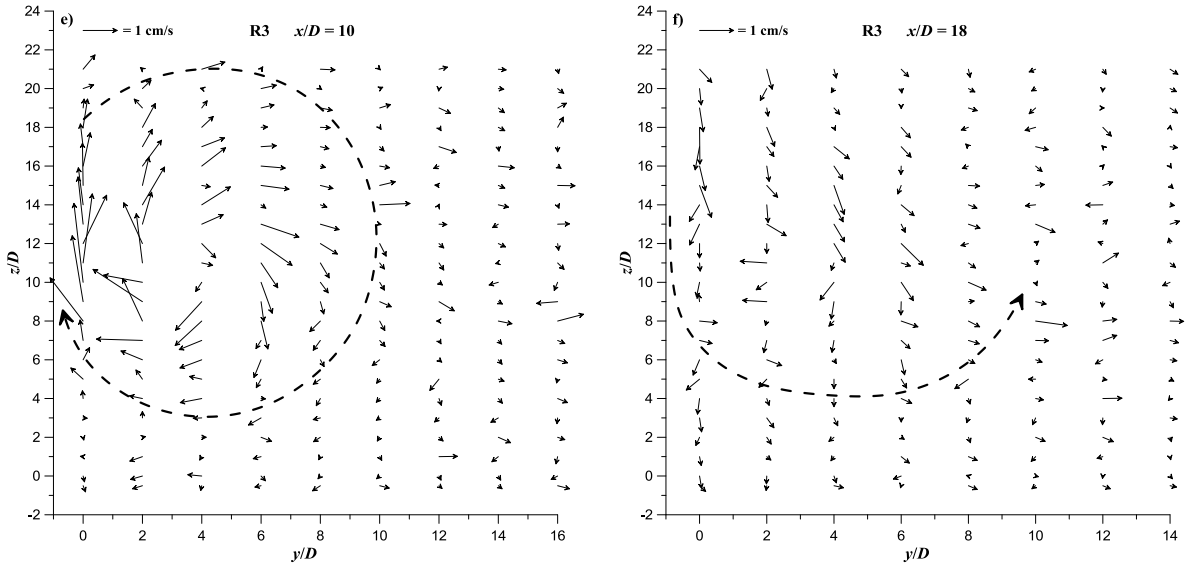


Fig. 8 Resultant velocity (V, W) distribution in the channel cross-section with the jet flow at x/D=10 (within the jet-ascending region) and 18 (within the jet-descending region).

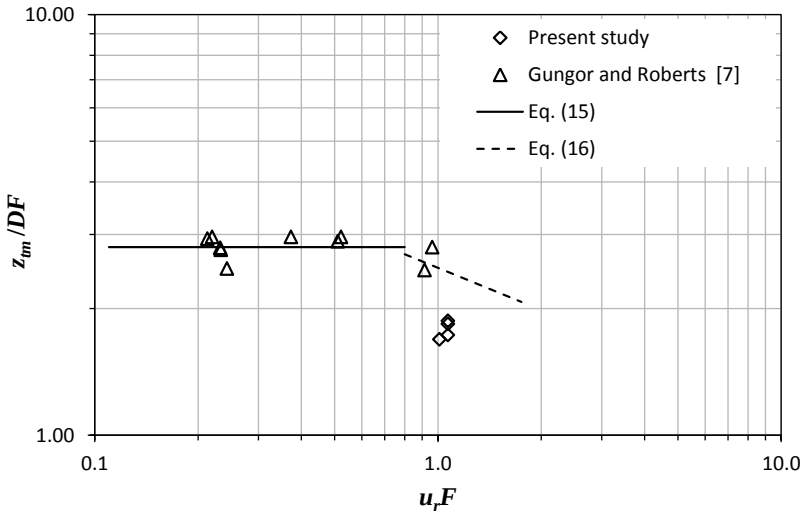


Fig. 9 Maximum jet rise height

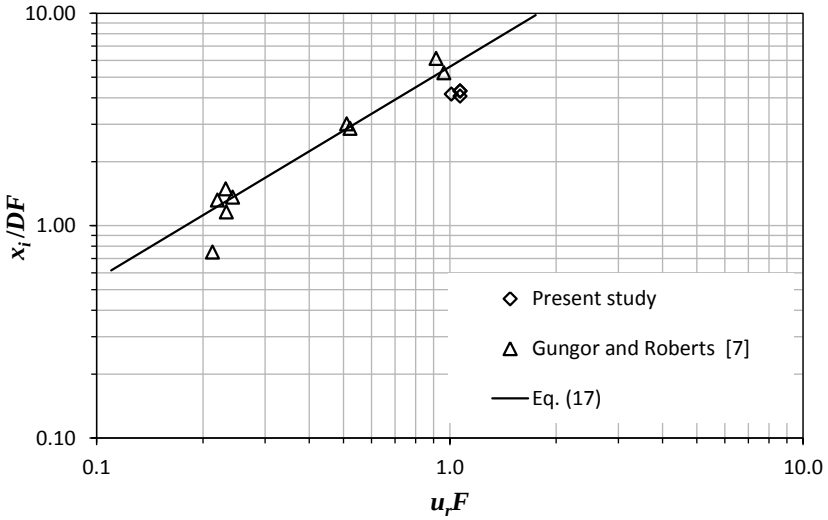


Fig. 10 Downstream position of the jet impact point

4. Conclusions

Dilution of brackish waters, that are discharged via single port or through a multiple port diffuser from osmotic power plants into a natural water body, is the most effective way to reduce environmental impacts. It is a complex process which is governed by the hydrodynamic conditions of miscible fluids of different proprieties. This paper focuses on the mixing processes that develop when a dense round jet outfall perpendicularly enters a shallow flowing current. The dense jet consisted of a salt water solution issued into a crossflow of fresh water. Extensive experimental measurements of both the salinity and the velocity flow fields were conducted to investigate the hydrodynamic jet behavior within the ambient current. In addition to examine the characteristic jet properties, i.e. its penetration within the surrounding ambient, its spreading and its dilution, in this study, special attention was also given to understand and confirm the conjecture, not yet experimentally demonstrated, of the development of the jet vortex structures, which are of specific patterns where dense jets are discharged into flowing currents.

The most significant results obtained in this study are summarized as follows.

The measured flow salinity and velocity fields clearly show the development of the dense jet within the flowing current. Results show that the dense jet is almost characterized by two distinct phases: a rapid ascent phase and a gradually descent phase. During the ascending phase, the jet behaves almost like a vertical pure jet discharged into a crossflow. Under the high momentum conditions, during this phase, the jet rapidly penetrates within the ambient flow. During the descending phase, however, the jet gradually descends under the buoyancy effects, extending longer downstream within the ambient flow until impacting the channel bottom. Downstream of the impact point, a bottom-spreading density current takes place.

The vertical profiles of the jet salinity are asymmetric between the upper and lower halves of the jet, above all in the ascending region. In the descending phase, this asymmetry is less pronounced and seems to vanish as going further downstream, giving rise to a symmetry distribution. The experimental results show that the jet undergoes a strong dilution during the initial rising phase. Over a downstream distance of order 6D, the jet salinity is approximately reduced by more than 85%. During the descending phase, the jet salinity continues to decrease (i.e. dilution continues to increase), but very gradually as going further downstream.

Based on the experimental results of the present study and the available data from existing literature, it is confirmed that the jet dilution increases as u_rF increases. The jet dilution at both the downstream positions x_t (at terminal rising height) and x_i (at impact point) is predictable as a function of u_rF.

Despite the numerous studies conducted on the understanding of the development of jet vortical structures, the generation and evolution of these structures are still misunderstood, constituting a challenge for any numerical simulation. The findings from this study provide insights into how the vortical structures develop and affect the mixing processes of a vertical dense jet discharged into a flowing current. In addition, the experimental results of this study certainly confirm the formation of the counter-rotating vortices pair in the descending region, which was not clear in other researches [7]. Furthermore, the measured flow velocity fields clearly suggest the development of such a structure also in the ascending region, which was not proved in previous studies [7]. Finally, it was observed that the counter-rotating vortices pair of the jet in the ascending and descending regions have opposite rotational direction. This finding is useful in clarifying the development process of vortical structures for dense jet, thusly improving numerical simulation accuracy.

Acknowledgement

This research was supported by a grant from the Italian national project "Hydroelectric energy by osmosis in coastal areas", PRIN 2010-2111. The experiments were carried out at the Coastal

Engineering Laboratory of the Dpt. of Civil, Environmental, Building Engineering and Chemistry, Technical University of Bari, Italy.

Notations

A_0	Jet source area (m^2)
B	Mean channel width (m)
B_0	Initial buoyancy flux ($m^4.s^{-3}$)
c	Local fluid conductivity ($S.m^{-1}$)
c_a	Ambient fluid conductivity ($S.m^{-1}$)
c_0	Initial jet fluid conductivity ($S.m^{-1}$)
C	dimensionless jet excess salinity (conductivity) (-)
D	Jet source diameter (m)
F	Jet densimetric Froude number (-)
g	Gravity acceleration ($m.s^{-2}$)
g'	Initial reduced gravity ($m.s^{-2}$)
H	Flow depth (m)
l_M	Jet-to-plume length scale (m)
l_m	Jet-to-crossflow length scale (m)
l_Q	Discharge length scale (m)
l_B	Plume-to-crossflow length scale (m)
M_0	Initial momentum flux ($m^4.s^{-2}$)
Q_0	Initial discharge volume flux ($m^3.s^{-1}$)
Re_0	Initial jet Reynolds number (-)
Ri_d	Richardson number (-)
S, s	Dilution (-)
S_i, s_i	Minimum dilution at the impact point (-)
S_t, s_t	Minimum dilution at the position of the terminal rise height (-)
U,V,W	Streamwise, spanwise and vertical time-averaged velocity (ms^{-1})
U_a	Mean ambient channel velocity ($m.s^{-1}$)
U_c	Velocity scale ($m.s^{-1}$)
U_0	Initial jet velocity ($m.s^{-1}$)
u_r	Ratio of ambient to jet velocity (-)
x, y, z	Longitudinal, lateral and vertical coordinates, respectively (m)
x_i	x-Position of the jet impact point (m)
x_t	x-Position at which the jet attains its maximum rising height (m)
z_L	Thickness of the bottom layer of the spreading density current (m)
z_{mt}	Jet terminal rise height (m)
z_t	Jet centerline rising height (m)
z_0	Jet port height (m)
$\Phi \cdot \cdot \Phi'$	Functions
ν_0	Initial jet kinematic viscosity ($m^2.s^{-1}$)
θ	**A**ngle relative to the horizontal (°)
ρ	Local fluid density ($kg.m^{-3}$)
ρ_a	Ambient fluid density ($kg.m^{-3}$)
ρ_0	Initial jet fluid density ($kg.m^{-3}$)

References

[1] Fischer HB, List EJ, Koh RCY, Imberger J, Brooks NH (1979) Mixing in inland and coastal waters. Academic, San Diego.

[2] Tong SS, Stolzenbach KD (1979) Submerged discharges of dense effluent. Rep No 243, Ralph M. Parsons Laboratory, Massachusetts Institute of Technology, Cambridge.

[3] Andreopoulos J, Rodi W (1984) Experimental investigation of jets in a crossflow. J Fluid Mech 138(1): 93-127. doi: 10.1017/S0022112084000057.

[4] Roberts P J W, Toms G (1987) Inclined dense jets in a flowing current. J Hydraul Eng 113(3): 323-341.

[5] Mossa M (2004) Experimental study on the interaction of non-buoyant jets and waves. J Hydraul Res 42(1): 13-28. doi: 10.1080/00221686.2004.9641179.

[6] Mossa M (2004) Behavior of nonbuoyant jets in a wave environment. J Hydraul Eng 130(7): 704-717. doi: 10.1061/(ASCE)0733-9429(2004)130:7(704).

[7] Gungor E, Roberts PJW (2009) Experimental Studies on Vertical Dense Jets in a Flowing Current. J Hydraul Eng ASCE 135(11): 935-948. doi: 10.1061/(ASCE)HY.1943-7900.0000106.

[8] Ben Meftah M, De Serio F, Malcangio D, Mossa M, Petrillo AF (2015) Experimental study of a vertical jet in a vegetated crossflow. J Environ Manage 164: 19-31. doi: 10.1016/j.jenvman.2015.08.035.

[9] Malcangio D, Mossa M (2016) A laboratory investigation into the influence of a rigid vegetation on the evolution of a round turbulent jet discharged within a cross flow. J Environ Manage 173: 105-120. doi:10.1016/j.jenvman.2016.02.044.

[10] Van der Zwan S, Pothof IWM, Blankert B, Bara JJ (2012) Feasibility of osmotic power from a hydrodynamic analysis at module and plant scale. J Membr Sci 389: 324-333.

[11] Achilli A, Cath TY, Childress A E (2009) Power generation with pressure retarded osmosis: an experimental and theoretical investigation. J Membr Sci 343: 42-52.

[12] Malcangio D, Ben Meftah M, Chiaia G, De Serio F, Mossa M, Petrillo AF (2016) Experimental Studies on Vertical Dense Jets in a Crossflow. Proc. River Flow 2016, USA, St. Louis Mo. 12-15 July (accepted).

[13] Montessori A, Prestininzi P, La Rocca M, Malcangio D, Mossa M. (2016) Two dimensional Lattice Boltzmann numerical simulation of a buoyant jet. Proc. 4th IAHR Europe Congress, Belgium, Liege 27-29 July, doi: 10.1201/b21902-165.

[14] Pedersen FB (1986) Environmental Hydraulics: stratified flows – Lecture notes on coastal and estuarine studies. Springer Verlag, Berlin.

[15] Platten JL, Keffer JF (1968) Entrainment in deflected axisymmetric jets at various angles to the stream. Tech Rep 6808, Dpt of Mech Eng, Univ of Toronto.

[16] Lai CCK, Lee JHW (2014) Initial mixing of inclined dense jets in perpendicular crossflows. Environl Fluid Mech 14(1): 25-49. doi: 10.1007/s10652-013-9290-7.

[17] Choi KW, Lai CCK, Lee JHW (2016) Mixing in the Intermediate Field of Dense Jets in Cross Currents. J Hydraul Eng ASCE 142 (1). doi:10.1061/(ASCE)HY.1943-7900.0001060

[18] Wang RQ, Law AWK, Adams EE (2011) Pinch-off and formation number of negatively buoyant jets. Phy Fluids 23(5): 052101. doi:10.1063/1.3584133.

[19] Wang RQ, Law AWK, Adams EE, Fringer OB (2009) Buoyant formation number of a starting buoyant jet. Phy Fluids 21: 125104. doi:10.1063/1.3275849.

[20] Cipollina A, Bonfiglio A, Micale G, Brucato A (2004) Dense jet modelling applied to the design of dense effluent diffusers. Desalination (167459-468). doi: 10.1016/j.desal.2004.06.161

[21] Abessi O, Roberts PJW (2016) Dense Jet Discharges in shallow water. J Hydraul Eng 142(1) 04015033 (1-13). doi: 10.1061/(ASCE)HY.1943-7900.0001057.

[22] Pincince AB, List EJ (1973) Disposal of brine into an estuary. J Water Pollut Control Fed 45: 2335–2344.

[23] Chu VH, Jirka GH (1986) Surface buoyant jets. Encyclopedia of Fluid Mechanic, Houston, Texas: Gulf Publishing Company.

[24] Abessi O, Saeedi M, Davidson M, Zaker NH (2012) Flow classification of negatively buoyant surface discharge in an ambient current. J Coast Res 278: 148-155. doi: 10.2112/JCOASTRES-D-10-00131.1.

[25] Ben Meftah M, De Serio F, Mossa M, Pollio A (2007) Analysis of the velocity field in a large rectangular channel with lateral shockwave. Environ. Fluid Mech. 7(6): 519-536. doi:10.1007/s10652-007-9034-7.

[26] Ben Meftah M, De Serio F, Mossa M, Pollio A (2008) Experimental study of recirculating flows generated by lateral shock waves in very large channels. Environ. Fluid Mech. 8(6): 215-238. doi:10.1007/s10652-008-9057-8.

[27] Ben Meftah M, Mossa M, Pollio A (2010) Considerations on shock wave/boundary layer interaction in undular hydraulic jumps in horizontal channels with a very high aspect ratio. Eur. J. Mech. - B/Fluids 29: 415-429. doi:10.1016/j.euromechflu.2010.07.002.

[28] Ben Meftah M, Mossa M (2013) Prediction of channel flow characteristics through square arrays of emergent cylinders. Phys. Fluids 25 (4): 045102, 1-21. doi:10.1063/1.4802047.

[29] Ben Meftah M, Mossa M (2016) A modified log-law of flow velocity distribution in partly obstructed open channels. Environ. Fluid Mech. 16(2): 453-479. doi:10.1007/s10652-015-9439-7.

[30] Ben Meftah M, De Serio F, Mossa M (2014) Hydrodynamic behavior in the outer shear layer of partly obstructed open channels, Phys. Fluids 26 (6), 065102, 1-19. doi: 10.1063/1.4881425.

[31] Malcangio D, Ben Meftah M, Mossa M (2016) Physical modelling of buoyant effluents discharged into a cross flow, Proc. IEEE Workshop on Environmental, Energy, and Structural Monitoring Systems, Italy, Bari 13-14 June, doi:10.1109/EESMS.2016.7504838.

[32] Besalduch LA, Badas MG, Ferrari S, Querzoli G (2013) Experimental Studies for the characterization of the mixing processes in negative buoyant jets. EPJ Web of Conferences 45, 01012 (1-9), doi: 10.1051/epjconf/20134501012.